surfaces

MDPI

Article

Slow Axisymmetric Migration of Multiple Colloidal Spheres with Slip Surfaces

Wei C. Lai and Huan J. Keh *

Department of Chemical Engineering, National Taiwan University, Taipei 10617, Taiwan; r13524124@ntu.edu.tw
* Correspondence: huan@ntu.edu.tw; Tel.: +886-2-33663048

Abstract

The quasi-steady low-Reynolds-number flow induced by a linear chain of multiple slip spheres translating along their common axis in a Newtonian fluid is investigated. The particles are allowed to differ in radius, Navier slip coefficient, migration velocity, and interparticle spacing. A semi-analytical solution of the governing Stokes equation is obtained using a boundary collocation method. Hydrodynamic interactions among the particles are shown to be significant under appropriate geometric and surface conditions. For the two-sphere configuration, the computed hydrodynamic forces agree closely with previously published asymptotic solutions derived via the twin multipole expansion method. In the three-sphere case, the presence of a third particle substantially modifies the forces acting on the other two, demonstrating non-negligible many-body interaction effects. The interaction strength is found to be more pronounced for smaller particles or those with lower slip coefficients. Calculations for longer particle chains further reveal a clear hydrodynamic shielding effect within the assembly.

Keywords: slip particle; axisymmetric translation; creeping flow; particle interaction; drag force

1. Introduction

The study of slow motions of colloidal particles in viscous fluids has long attracted significant attention across various fields of science, technology, and engineering. Although creeping-flow particle migration is fundamentally theoretical in nature, it plays a crucial role in numerous applications, including coagulation, sedimentation, flotation, suspension rheology, microfluidic transport, and various phoretic processes. The analysis of low-Reynolds-number particle motion originates from Stokes' pioneering work on the steady translation of a rigid no-slip sphere in a Newtonian fluid [1]. While the no-slip boundary condition is traditionally assumed in creeping-flow problems, deviations from this condition arise in several practical systems. In particular, slip boundary behavior has been reported for lyophobic particles [2–6], aerosol particles [7–9], and porous particles [10,11]. Under the Navier slip model, the local tangential slip velocity at the particle surface is proportional to the viscous shear stress, with the proportionality determined by the slip coefficient β^{-1} [12–15].

The hydrodynamic force acting on a slip spherical particle with radius a translating at velocity U in a fluid with viscosity η was determined as [16]

Academic Editor: Gaetano Granozzi

Received: 24 March 2026
Revised: 15 April 2026
Accepted: 20 April 2026
Published: 23 April 2026

 https://doi.org/10.3390/surfaces9020038

$$F^{(0)} = -6\pi\eta a U \frac{\beta a + 2\eta}{\beta a + 3\eta}, \tag{1}$$

where η/β indicates a slip length [12,17]. In the limit with infinite stickiness parameter ($\beta a/\eta \to \infty$), the particle is no-slip and Equation (1) reduces to Stokes' law. In the other limit with $\beta a/\eta = 0$, the particle is fully slip and identical to an inviscid gas bubble in liquids.

In realistic systems, particles rarely migrate in isolation. Consequently, hydrodynamic interactions between neighboring slip particles must be carefully evaluated [18,19]. The axisymmetric slow migration of two slip spheres has previously been examined using exact representations in spherical bipolar coordinates, covering both identical [20] and non-identical [21,22] particle configurations. Alternative analytical approaches, including twin multipole expansions, have been developed for two arbitrarily oriented slip spheres [23]. More recently, boundary collocation techniques have also been applied to investigate coaxial migration of two arbitrary slip spheres [24]. These studies consistently demonstrate that hydrodynamic interaction decreases as the slip coefficient increases, intensifies as the interparticle gap narrows, and tends to be stronger for smaller particles.

In concentrated suspensions or structured particle assemblies, many-body interactions may become particularly important. Although there are many studies in the literature on the interaction of two slowly moving slip particles, there are no studies on the interaction of three or more translating slip particles. The present study extends prior two-particle analyses to a linear chain of multiple coaxial slip spheres migrating slowly along their line of centers. The particles may differ in size, slip coefficient, velocity, and spacing. The Stokes equation is solved semi-analytically using the boundary collocation method, yielding highly convergent solutions for the hydrodynamic forces acting on each particle. For the two-sphere limit, the computed forces agree well with previously reported numerical [22] and asymptotic [23] results, thereby validating the present formulation.

2. Analysis

We consider the pseudo-steady creeping flow caused by a linear chain of N slip spheres translating along their line of centers (z axis) in an unbounded, incompressible, Newtonian fluid with viscosity η at rest at infinity, as illustrated in Figure 1. The origin of the spherical coordinates (r_i, θ_i, ϕ) is set at the center of the sphere i, where $i = 1, 2, \ldots$, and N, and the cylindrical coordinates (ρ, ϕ, z) are measured from the center of the first sphere. The goal is to obtain the correction value for the translation of each sphere in Equation (1) due to the presence of other spheres.

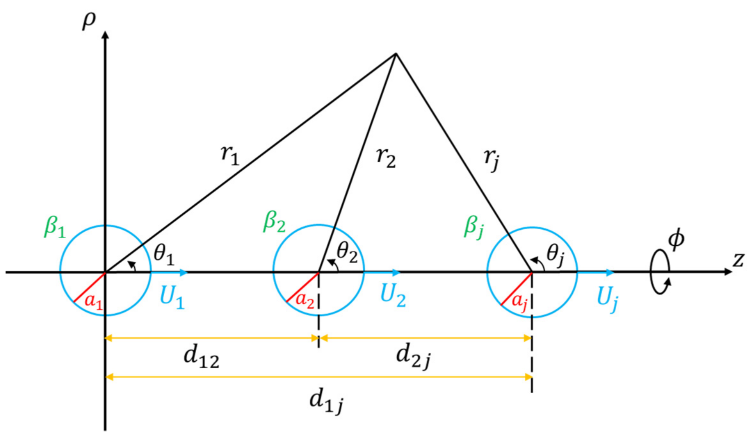

Figure 1. Geometrical sketch of the axisymmetric migration of a chain of multiple spherical particles.

Assume that the Reynolds number is low (less than about 0.1). Thus, the fluid velocity is governed by the Stokes equation for the axisymmetric flow,

$$E^2(E^2\Psi) = 0, \tag{2}$$

where Ψ is the stream function, which satisfies the continuity equation immediately and is related to the non-zero fluid velocity components by

$$v_\rho = \frac{1}{\rho}\frac{\partial\Psi}{\partial z}, \quad v_z = -\frac{1}{\rho}\frac{\partial\Psi}{\partial\rho} \tag{3}$$

and the Stokes operator

$$E^2 = \rho\frac{\partial}{\partial\rho}(\frac{1}{\rho}\frac{\partial}{\partial\rho}) + \frac{\partial^2}{\partial z^2}. \tag{4}$$

Because the local slip velocity of the fluid is proportional to the essential shear stress at the surface of each solid sphere (the Navier slip model is employed) [12,16] and the fluid is at rest at infinity, the boundary conditions for the velocity field are

$$r_i = a_i: \quad v_\rho = \frac{1}{\beta_i}\tau_{r_i\theta_i}\cos\theta_i, \quad v_z = U_i - \frac{1}{\beta_i}\tau_{r_i\theta_i}\sin\theta_i, \tag{5}$$

$$(\rho^2+z^2)^{1/2} \to \infty: \quad v_\rho = v_z = 0, \tag{6}$$

where

$$\tau_{r_i\theta_i} = \eta[r_i\frac{\partial}{\partial r_i}(\frac{v_{\theta_i}}{r_i}) + \frac{1}{r_i}\frac{\partial v_{r_i}}{\partial\theta_i}], \tag{7}$$

and a_i, U_i, and $1/\beta_i$ are the radius, velocity, and Navier slip coefficient of the sphere i.

A general solution to Equations (2)–(4) of the fluid flow immediately satisfying Boundary Condition (6) at infinity is [7,25,26]

$$\Psi = \sum_{j=1}^{N}\sum_{n=2}^{\infty}[(B_{jn}r_j^{-n+1} + D_{jn}r_j^{-n+3})G_n^{-1/2}(\cos\theta_j)], \tag{8}$$

$$v_\rho = \sum_{j=1}^{N}\sum_{n=2}^{\infty}[B_{jn}B'_n(r_j,\theta_j) + D_{jn}D'_n(r_j,\theta_j)], \tag{9}$$

$$v_z = \sum_{j=1}^{N}\sum_{n=2}^{\infty}[B_{jn}B''_n(r_j,\theta_j) + D_{jn}D''_n(r_j,\theta_j)], \tag{10}$$

where

$$B'_n(r_j,\theta_j) = -r_j^{-n-1}(n+1)G_{n+1}^{-1/2}(\cos\theta_j)\csc\theta_j, \tag{11}$$

$$D'_n(r_j,\theta_j) = -r_j^{-n+1}[(n+1)G_{n+1}^{-1/2}(\cos\theta_j)\csc\theta_j - 2G_n^{-1/2}(\cos\theta_j)\cot\theta_j], \tag{12}$$

$$B''_n(r_j,\theta_j) = -r_j^{-n-1}P_n(\cos\theta_j), \tag{13}$$

$$D''_n(r_j,\theta_j) = -r_j^{-n+1}[P_n(\cos\theta_j) + 2G_n^{-1/2}(\cos\theta_j)], \tag{14}$$

$j = 1, 2, \ldots$, and N, $G_n^{-1/2}$ and P_n are the Gegenbauer function (with degree $-1/2$) and Legendre function, respectively, of the first kind of order n, and the unknown coefficients B_{jn} and D_{jn} will be determined using Equation (5). When constructing solutions in Equations (8)–(10), due to the linearity of Equation (2), the superposition of its general solutions in spherical coordinate systems written from N different origins can be used.

Substituting Equations (9) and (10) into Equation (5), we obtain

$$\sum_{j=1}^{N}\sum_{n=2}^{\infty}\{B_{jn}[B'_n(r_j,\theta_j)-\frac{\eta}{\beta_i}\cos\theta_i\alpha_{in}(r_j,\theta_j)]+D_{jn}[D'_n(r_j,\theta_j)$$

$$-\frac{\eta}{\beta_i}\cos\theta_i\gamma_{in}(r_j,\theta_j)]\}_{r_i=a_i}=0, \quad (15)$$

$$\sum_{j=1}^{N}\sum_{n=2}^{\infty}\{B_{jn}[B''_n(r_j,\theta_j)+\frac{\eta}{\beta_i}\sin\theta_i\alpha_{in}(r_j,\theta_j)]+D_{jn}[D''_n(r_j,\theta_j)$$

$$+\frac{\eta}{\beta_i}\sin\theta_i\gamma_{in}(r_j,\theta_j)]\}_{r_i=a_i}=U_i, \quad (16)$$

where

$$\alpha_{in}(r_j,\theta_j)=r_j^{-n-2}[E_n^*(\theta_j)\cos\theta_i\sin\theta_i+E_n^{**}(\theta_j)(\cos^2\theta_i-\sin^2\theta_i)\Big] \quad (17)$$

$$\gamma_{in}(r_j,\theta_j)=r_j^{-n}[H_n^*(\theta_j)\cos\theta_i\sin\theta_i+H_n^{**}(\theta_j)(\cos^2\theta_i-\sin^2\theta_i)] \quad (18)$$

$$E_n^*(\theta_j)=2[(n+1)(n+\csc^2\theta_j)G_{n+1}^{-1/2}(\cos\theta_j)$$

$$-(3n+2)P_n(\cos\theta_j)\cos\theta_j+nP_{n-1}(\cos\theta_j)] \quad (19)$$

$$E_n^{**}(\theta_j)=n[(n+1)G_{n+1}^{-1/2}(\cos\theta_j)+P_{n-1}(\cos\theta_j)]\cot\theta_j$$

$$+[(3n+2)\sin\theta_j-n\csc\theta_j]P_n(\cos\theta_j) \quad (20)$$

$$H_n^*(\theta_j)=2[(n+1)(n-1+\cot^2\theta_j)G_{n+1}^{-1/2}(\cos\theta_j)-2(2n-1+\cot^2\theta_j)G_n^{-1/2}(\cos\theta_j)\cos\theta_j$$

$$+(n+2-4\sin^2\theta_j)P_{n-1}(\cos\theta_j)-3nP_n(\cos\theta_j)\cos\theta_j] \quad (21)$$

$$H_n^{**}(\theta_j)=2[2(n-1)\sin\theta_j-(n-2)\csc\theta_j]G_n^{-1/2}(\cos\theta_j)+(n^2-n-2)G_{n+1}^{-1/2}(\cos\theta_j)\cot\theta_j$$

$$+(n-4\sin^2\theta_j)P_{n-1}(\cos\theta_j)\cot\theta_j+n(3\sin\theta_j-\csc\theta_j)P_n(\cos\theta_j) \quad (22)$$

Equations (8)–(22) can be expressed in coordinates (ρ,z) using the following conversion formulas:

$$r_j=[(z-d_{1j})^2+\rho^2]^{1/2}, \qquad \theta_j=\cos^{-1}(\frac{z-d_{1j}}{r_j}), \quad (23)$$

where d_{ij} denotes the center-to-center distance of the spheres i and j with $d_{jj}=0$ obviously.

The boundary collocation method [7,25,26] lets the boundary conditions in Equations (15) and (16) be satisfied at M points evenly distributed along the longitudinal semicircle of each spherical surface (with $r_i=a_i$) and their infinite series be truncated after the first M terms, resulting in $2MN$ algebraic equations in the truncated form. For necessarily large number of M, these simultaneous equations can be solved numerically to lead to the $2MN$ unknown coefficients B_{jn} and D_{jn} required in the truncated versions of Equations (9) and (10) for the fluid velocity field.

The drag force exerted by the fluid on the sphere i can be determined from [12,25]

$$F_i=4\pi\eta D_{i2} \quad (24)$$

which indicates that only the lowest-order coefficient D_{i2} contributes to the drag force F_i. This force result can be expressed by

$$F_i = \sum_{j=1}^{N} h_{ij} F_j^{(0)}, \tag{25}$$

where

$$F_j^{(0)} = -6\pi\eta a_j U_j \frac{1 + 2\eta/\beta_j a_j}{1 + 3\eta/\beta_j a_j}, \tag{26}$$

which is the hydrodynamic force exerted on the sphere j in the absence of the other spheres given by Equation (1), and the force correction parameters h_{ij} depend on the nondimensionalized radii, spacings, and slip coefficients of the spheres. Evidently, h_{ij} is equal to unity if $j = i$ and nil if $j \neq i$ as the spacings are infinite.

3. Results of Two Slip Spheres

The boundary collocation results for the axisymmetric translation of two spherical particles ($N = 2$) are presented in this section. Once unknown coefficients B_{1n}, D_{1n}, B_{2n}, and D_{2n} in Equations (8)–(10) for the fluid flow field are solved using the truncated versions of Equations (15) and (16), the drag forces acting on each sphere can be calculated using Equation (24). Table 1 presents the numerical results of four force correction parameters (h_{11}, h_{12}, h_{21}, and h_{22}) in Equation (25) for two identical slip particles (with $\beta_1 = \beta_2 = \beta$, $a_1 = a_2 = a$, $h_{12} = h_{21}$, and $h_{11} = h_{22}$) with different values of spacing parameter $2a/d_{12}$ and stickiness/slip parameter $\beta a/\eta$. Table 2 gives the collocation results of these four force correction parameters for the axisymmetric translation of two no-slip particles ($\beta_1 \to \infty$ and $\beta_2 \to \infty$) with dissimilar radii (a_2/a_1 equals 2 and 5) under several values of spacing parameter $(a_1 + a_2)/d_{12}$. Table 3 presents the collocation solutions of these force correction parameters for the case where the two particles differ in radius or slip coefficient under different values of $(a_1 + a_2)/d_{12}$. Our numerical solutions converge to at least five decimal places.

Table 1. Force correction parameters h_{11}, h_{12}, h_{21}, and h_{22} for the axially symmetric translation of two identical slip particles ($\beta_1 = \beta_2 = \beta$ and $a_1 = a_2 = a$). The asymptotic solutions are calculated using Equations (27)–(43) for comparison.

$\frac{\beta a}{\eta}$	$\frac{2a}{d_{12}}$	Collocation Solutions		Asymptotic Solutions	
		$h_{11} = h_{22}$	$-h_{12} = -h_{21}$	$h_{11} = h_{22}$	$-h_{12} = -h_{21}$
0	0.1	1.00251	0.05013	1.00251	0.05013
	0.2	1.01021	0.10103	1.01010	0.10101
	0.3	1.02357	0.15362	1.02303	0.15346
	0.4	1.04356	0.20909	1.04173	0.20836
	0.5	1.07182	0.26924	1.06689	0.26678
	0.6	1.11125	0.33704	1.09954	0.33008
	0.7	1.16741	0.41814	1.14113	0.40004
	0.8	1.25302	0.52537	1.19364	0.47910
	0.9	1.40919	0.70011	1.25969	0.57064
	0.99	1.96370	1.26906	1.33353	0.66749
	0.999	2.53450	1.84122	1.34178	0.67849
1	0.1	1.00318	0.05640	1.00318	0.05640
	0.2	1.01291	0.11372	1.01291	0.11372
	0.3	1.02979	0.17304	1.02978	0.17306
	0.4	1.05499	0.23585	1.05493	0.23600
	0.5	1.09053	0.30440	1.09016	0.30504
	0.6	1.14003	0.38252	1.13822	0.38443
	0.7	1.21049	0.47748	1.20309	0.48130
	0.8	1.31814	0.60590	1.29041	0.60731
	0.9	1.51631	0.82165	1.40787	0.78097
	0.99	2.23845	1.55735	1.54780	1.00108
	0.999	2.99768	2.31783	1.56395	1.02752

Table 1. *Cont.*

$\frac{\beta a}{\eta}$	$\frac{2a}{d_{12}}$	Collocation Solutions		Asymptotic Solutions	
		$h_{11} = h_{22}$	$-h_{12} = -h_{21}$	$h_{11} = h_{22}$	$-h_{12} = -h_{21}$
10	0.1	1.00482	0.06947	1.00482	0.06947
	0.2	1.01962	0.14043	1.01962	0.14043
	0.3	1.04547	0.21474	1.04546	0.21474
	0.4	1.08451	0.29505	1.08437	0.29504
	0.5	1.14054	0.38571	1.13966	0.38550
	0.6	1.22071	0.49447	1.21640	0.49279
	0.7	1.33986	0.63698	1.32207	0.62762
	0.8	1.53524	0.85146	1.46727	0.80669
	0.9	1.94195	1.27396	1.66667	1.05550
	0.99	3.85846	3.20253	1.90863	1.36993
	0.999	6.22441	5.56958	1.93680	1.40754
∞	0.1	1.00566	0.07530	1.00566	0.07530
	0.2	1.02310	0.15250	1.02310	0.15250
	0.3	1.05380	0.23401	1.05378	0.23401
	0.4	1.10073	0.32349	1.10050	0.32340
	0.5	1.16947	0.42721	1.16790	0.42646
	0.6	1.27112	0.55714	1.26322	0.55262
	0.7	1.43103	0.73975	1.39723	0.71714
	0.8	1.72267	1.04975	1.58541	0.94408
	0.9	2.49543	1.83763	1.84928	1.27021
	0.99	14.25276	13.60645	2.17541	1.69324
	0.999	127.26061	126.61536	2.21369	1.74439

Table 2. Force correction parameters h_{11}, h_{12}, h_{21}, and h_{22} for the axially symmetric translation of two nonslip particles ($\beta_1 \to \infty$ and $\beta_2 \to \infty$). The values in parentheses are asymptotic solutions calculated using Equations (27)–(39) for comparison.

$\frac{a_2}{a_1}$	$\frac{a_1+a_2}{d_{12}}$	h_{11}	$-h_{12}$	$-h_{21}$	h_{22}
2	0.2	1.02072 (1.02072)	0.10133 (0.10133)	0.20266 (0.20266)	1.02026 (1.02026)
	0.4	1.09297 (1.09269)	0.21267 (0.21262)	0.42535 (0.42524)	1.08483 (1.08468)
	0.6	1.26329 (1.25409)	0.35908 (0.35635)	0.71815 (0.71270)	1.21279 (1.20777)
	0.8	1.75811 (1.59763)	0.65583 (0.59258)	1.31172 (1.18516)	1.51063 (1.42587)
	0.9	2.65282 (1.89200)	1.12447 (0.78603)	2.24895 (1.57207)	1.98411 (1.59220)
	0.99	16.58479 (2.26502)	8.10827 (1.03550)	16.21630 (2.07099)	8.97381 (1.78994)
	0.999	150.50332 (2.30929)	75.06912 (1.06560)	150.13823 (2.13121)	75.93531 (1.81276)
5	0.2	1.01301 (1.01301)	0.05016 (0.05016)	0.25082 (0.25082)	1.01244 (1.01244)
	0.4	1.05936 (1.05913)	0.10190 (0.10188)	0.50950 (0.50941)	1.04930 (1.04925)
	0.6	1.17392 (1.16648)	0.16126 (0.16037)	0.80631 (0.80187)	1.11177 (1.11018)
	0.8	1.53365 (1.40491)	0.26252 (0.24206)	1.31267 (1.21029)	1.22658 (1.19918)
	0.9	2.22149 (1.61470)	0.41189 (0.30332)	2.05942 (1.51661)	1.38389 (1.25815)
	0.99	13.16540 (1.88453)	2.60972 (0.37966)	13.04862 (1.89831)	3.58867 (1.32291)
	0.999	117.92895 (1.91677)	23.56325 (0.38877)	117.81627 (1.94384)	24.54287 (1.33013)

Table 3. Force correction parameters (h_{11}, h_{12}, h_{21}, and h_{22}) for the axially symmetric translation of two particles with a different in radius or stickiness.

$\frac{a_1+a_2}{d_{12}}$	h_{11}	$-h_{12}$	$-h_{21}$	h_{22}
		$a_2/a_1 = 1$, $\beta_1 a_1/\eta = 1$, $\beta_2 \to \infty$		
0.1	1.00425	0.05643	0.07524	1.00424
0.2	1.01730	0.11396	0.15195	1.01721
0.3	1.04023	0.17396	0.23194	1.03971
0.4	1.07508	0.23837	0.31783	1.07333
0.5	1.12561	0.31037	0.41383	1.12089
0.6	1.19891	0.39570	0.52761	1.18775
0.7	1.31005	0.50622	0.67496	1.28525
0.8	1.49885	0.67255	0.89674	1.44335
0.9	1.93216	1.02072	1.36096	1.78745
0.99	6.51766	4.48010	5.97347	5.24638
0.999	44.89054	33.26178	44.34904	34.02817
		$a_2/a_1 = 2$, $\beta_1 a_1/\eta = 3$, $\beta_2 = \beta_1$		
0.1	1.00373	0.04177	0.08910	1.00371
0.2	1.01525	0.08416	0.17954	1.01496
0.3	1.03562	0.12795	0.27297	1.03412
0.4	1.06690	0.17428	0.37179	1.06192
0.5	1.11283	0.22496	0.47991	1.09976
0.6	1.18021	0.28326	0.60429	1.15033
0.7	1.28280	0.35573	0.75890	1.21945
0.8	1.45357	0.45801	0.97708	1.32190
0.9	1.80601	0.64353	1.37287	1.51024
0.99	3.34373	1.38123	2.94661	2.25211
0.999	5.12212	2.21647	4.72846	3.08784

For any combination of $\beta_1 a_1/\eta$, $\beta_2 a_2/\eta$, and a_2/a_1 in Tables 1–3, both the force correction parameters h_{11} and h_{22} are positive increasing functions of the spacing parameter $(a_1 + a_2)/d_{12}$ and equal to unity as $(a_1 + a_2)/d_{12} = 0$, whereas both h_{12} and h_{21} are negative with their magnitudes increasing with $(a_1 + a_2)/d_{12}$ but vanishing as $(a_1 + a_2)/d_{12} = 0$. These results, which agree well with those obtained by using spherical bipolar coordinates [22], indicate that the interaction between particles increases as the thickness of the gap between particles decreases. This interaction is generally very important when $(a_1 + a_2)/d_{12} \to 1$, and for any given value of $(a_1 + a_2)/d_{12}$, it affects a larger or more slippery (less sticky) sphere less than a smaller or less slippery (more sticky) sphere.

A twin multipole expansion method was used to obtain the following power series formulae of the four force correction parameters for the axisymmetric translation of two slip spherical particles when $\beta_2 a_2 = \beta_1 a_1 = \beta a$ [23]:

$$h_{12}(s,\lambda) = h_{21}(s,\lambda^{-1}) = -\lambda^{-1}\sum_{k=0}^{\infty} s^{-2k-1} f_{2k+1}(\lambda)(1+\lambda)^{-2k-1}, \tag{27}$$

$$h_{11}(s,\lambda) = h_{22}(s,\lambda^{-1}) = \sum_{k=0}^{\infty} s^{-2k} f_{2k}(\lambda)(1+\lambda)^{-2k}, \tag{28}$$

where $\lambda = a_2/a_1$, $s = 2d_{12}/(a_1 + a_2)$,

$$f_0 = 1, \quad f_1 = 3\beta_{23}\lambda, \quad f_2 = 9\beta_{23}^2\lambda, \quad f_3 = -4\beta_{03}\lambda(1+\lambda^2) + 27\beta_{23}^3\lambda^2, \tag{29}$$

$$f_4 = -24\beta_{03}\beta_{23}\lambda + 81\beta_{23}^4\lambda^2 + 36w(10)\beta_{03}\beta_{05}\beta_{23}\lambda^3, \tag{30}$$

$$f_5 = 72w(15)\beta_{03}\beta_{05}\beta_{23}^2\lambda^2(1+\lambda^2) + 243\beta_{23}^5\lambda^3, \tag{31}$$

$$f_6 = 16\beta_{03}^2\lambda + 108w(30)\beta_{03}\beta_{05}\beta_{23}^3\lambda^2 + (32\beta_{03}^2 - 480\beta_{05}\beta_{23} + 729\beta_{23}^6)\lambda^3$$
$$+648w(10)\beta_{03}\beta_{05}\beta_{23}^3\lambda^4 + \frac{144}{5}[\beta_{(-2)3} - 10\beta_{05} + 14\beta_{27}]\beta_{23}\lambda^5, \tag{32}$$

$$f_7 = \frac{144}{5}[3\beta_{(-2)3} + 42\beta_{27} - 35w(\frac{46}{7})\beta_{02}\beta_{03}\beta_{05}]\beta_{23}^2\lambda^2(1+\lambda^4)$$
$$+1620w(12)\beta_{03}\beta_{05}\beta_{23}^4\lambda^3(1+\lambda^2)$$
$$+3[64\beta_{03}^2 - 720\beta_{05}\beta_{23} + 729\beta_{23}^6 + 48w(10)(10\beta_{05}\beta_{23} - \beta_{03}^2)]\beta_{23}\lambda^4; \tag{33}$$

$$\beta_{nm} = \frac{\beta a + n\eta}{\beta a + m\eta}, \tag{34}$$

$$w(x) = 1 + 5\frac{\eta}{\beta a} + x(\frac{\eta}{\beta a})^2. \tag{35}$$

Therefore, for the whole range $0 \le \lambda < \infty$, there are only two independent force correction parameters that need to be determined. Instead, we can determine all four force correction parameters within the half range $1 \le \lambda < \infty$. For the special case of $\beta_1 \to \infty$ and $\beta_2 \to \infty$ (two no-slip particles), further $f_k(\lambda)$ terms can be obtained [27]:

$$f_8 = 3[192\lambda^2(1+\lambda^5) + 1616\lambda^3 + 1803\lambda^4 + 1508\lambda^5 + 1296\lambda^6], \tag{36}$$

$$f_9 = 1152\lambda^2(1+\lambda^6) + 9072\lambda^3(1+\lambda^4) + 14{,}752\lambda^4(1+\lambda^2) + 26{,}163\lambda^5, \tag{37}$$

$$f_{10} = 2304\lambda^2(1+\lambda^7) + 20{,}736\lambda^3(1+\lambda^5) + 42{,}804\lambda^4 + 115{,}849\lambda^5$$
$$+76{,}176\lambda^6 + 39{,}264\lambda^7, \tag{38}$$

$$f_{11} = 3[1536\lambda^2(1+\lambda^8) + 15{,}552\lambda^3(1+\lambda^6) + 36{,}304\lambda^4(1+\lambda^4)$$
$$+89{,}700\lambda^5(1+\lambda^2) + 106{,}633\lambda^6]. \tag{39}$$

On the other hand, for the special case of $\beta_1 \to 0$ and $\beta_2 \to 0$ (two perfect slip particles or gas bubbles), further $f_k(\lambda)$ terms can also be obtained [23]:

$$f_8 = \frac{512}{3}(\lambda^2 + 2\lambda^3 + 5\lambda^4 + 3\lambda^5 + 3\lambda^6 + \lambda^7), \tag{40}$$

$$f_9 = \frac{1024}{3}(\lambda^2 + 3\lambda^3 + 6\lambda^4 + 8\lambda^5 + 6\lambda^6 + 3\lambda^7 + \lambda^8), \tag{41}$$

$$f_{10} = \frac{2048}{3}(\lambda^2 + 3\lambda^3 + 9\lambda^4 + 11\lambda^5 + 14\lambda^6 + 6\lambda^7 + 4\lambda^8 + \lambda^9), \tag{42}$$

$$f_{11} = \frac{4096}{3}(\lambda^2 + 4\lambda^3 + 10\lambda^4 + 20\lambda^5 + 21\lambda^6 + 20\lambda^7 + 10\lambda^8 + 4\lambda^9 + \lambda^{10}). \tag{43}$$

Tables 1 and 2 also list the asymptotic solutions of the four force correction parameters calculated using the above formulae for comparison. When $(a_1 + a_2)/d_{12}$ is small, our collocation solutions agree well with these asymptotic results. However, when $(a_1 + a_2)/d_{12}$ approaches unity, the errors in these asymptotic results turn out to be significant.

For the axisymmetric translation of two slip spherical particles with $\beta_2 a_2 = \beta_1 a_1$, the formula $h_{21}a_1 = h_{12}a_2$ can be obtained by using the reciprocal theorem of Lorentz [13]. The collocation solutions in Tables 1 and 2 satisfy this formula and the relationships $h_{11} + h_{21} \le 1$ and $h_{12} + h_{22} \le 1$ (where h_{11} and h_{22} are positive but h_{12} and h_{21} are negative). Thus, the translation of a sphere is enhanced (the drag force is abridged) by another neighboring sphere translating in the same direction at a comparable or greater velocity but is hindered (the drag force is increased) by another sphere translating in the opposite direction at an arbitrary velocity.

4. Results of Multiple Slip Spheres

In this section, we present the boundary collocation solutions for the axisymmetric translation of a linear chain of three or more slip spherical particles. According to Equation (25), the general problem of a three-sphere chain would require nine correction parameters to characterize the drag forces. For simplicity, we will only consider the translational motion of three particles with the same slip coefficient in symmetric arrangement; that is, the particles at the two ends of the chain have equal radii and are equidistant from the center particle ($\beta_1 = \beta_2 = \beta_3 = \beta$, $a_1 = a_3$, and $d_{12} = d_{23} = d$). In this case, there are obviously some equations relating the force correction parameters:

$$h_{33} = h_{11},\ h_{32} = h_{12},\ h_{23} = h_{21},\ h_{31} = h_{13}. \quad (44)$$

Table 4 presents the collocation solutions of the force correction parameters in Equation (25) when three identical particles (with $a_1 = a_2 = a_3 = a$) translate under various values of spacing parameter $2a/d$ and stickiness parameter $\beta a/\eta$. Table 5 shows the collocation solutions of these force correction parameters for two relative particle radii (a_2/a_1 equals 1/2 and 2) when three no-slip particles ($\beta \to \infty$) translate under different values of spacing parameter $(a_1 + a_2)/d$. Table 6 presents the collocation solutions of these force correction parameters when three particles translate under $\beta a_2/\eta = 1$, $a_2/a_1 = 1/2$ and 2, and different values of $(a_1 + a_2)/d$. Again, h_{ij} are positive if $j = i$ and negative if $j \neq i$. The particle-particle interaction generally increases as the spacing between neighboring particles decreases. However, as shown in Table 6, when the center particle is larger than the end particles, the force correction parameters h_{31} and h_{13} are not always monotonic functions of $(a_1 + a_2)/d$. Likewise, in Tables 4 and 5, the formula $h_{21}a_1 = h_{12}a_2$ obtained from the reciprocal theorem of Lorentz applies to the translation of the three-particle chain with $\beta_2 a_2 = \beta_1 a_1$, and for a specified value of $(a_1 + a_2)/d$, the particle interaction effect on drag forces is weaker for larger or more slippery particles than for smaller or less slippery particles.

Understanding the impact of a third particle's presence on the drag forces of its two adjacent particles can be meaningful. In Figure 2, we plot the normalized drag forces $F_i/F^{(0)}$ as functions of spacing parameter $2a/d$ with solid curves when three identical and equally spaced particles ($a_1 = a_2 = a_3 = a$, $\beta_1 = \beta_2 = \beta_3 = \beta$, and $d_{12} = d_{23} = d$) translate along their centerline at the same velocity ($U_1 = U_2 = U_3 = U$ and $F_1^{(0)} = F_2^{(0)} = F_3^{(0)} = F^{(0)}$) for different values of stickiness parameter $\beta a/\eta$. For comparison, in the same figure, we plot the corresponding result of the normalized drag forces experienced by the first and second spheres in the absence of a third sphere with dashed curves. Evidently, the presence of the third sphere significantly reduces the drag forces experienced by the other two spheres. The drag force reduction is much greater for the central sphere than for the spheres at the two ends, as expected. As illustrated in Figure 2a (and Tables 1 and 4), when no-slip spheres ($\beta \to \infty$) are almost in contact ($2a/d = 0.999$), the presence of a third sphere reduces the drag force on the first (other end) sphere by only about 7%. Conversely, as illustrated in Figure 2b, when these spheres are almost in contact, the drag force on the second (central) sphere is abridged by as much as about 45%. Due to the symmetry of configuration, the drag force generated by two identical spherical particles, as shown in Figure 2 and Table 1, when they are separated by a distance d and translated at equal but opposite velocities is the same as the drag force generated by an isolated spherical particle translating at the same velocity perpendicular to an infinite free surface plane at a distance $d/2$.

https://doi.org/10.3390/surfaces9020038

Table 4. Force correction parameters for the translation of three identical spherical particles with equal spacings ($\beta_1 = \beta_2 = \beta_3 = \beta$, $a_1 = a_2 = a_3 = a$, and $d_{12} = d_{23} = d$).

$\beta a/\eta$	$\frac{2a}{d}$	h_{22}	$h_{11} = h_{33}$	$-h_{12} = -h_{32} = -h_{21} = -h_{23}$	$-h_{13} = -h_{31}$
1	0.1	1.00620	1.00381	0.05502	0.02514
	0.2	1.02472	1.01490	0.10887	0.04499
	0.3	1.05633	1.03333	0.16342	0.06042
	0.4	1.10316	1.05992	0.22070	0.07227
	0.5	1.16930	1.09657	0.28335	0.08134
	0.6	1.26213	1.14687	0.35549	0.08840
	0.7	1.39596	1.21789	0.44458	0.09409
	0.8	1.60357	1.32592	0.56733	0.09895
	0.9	1.99191	1.52438	0.77767	0.10328
	0.99	3.42890	2.24669	1.50876	0.10683
	0.999	4.94273	3.00390	2.26684	0.10709
10	0.1	1.00936	1.00572	0.06744	0.03016
	0.2	1.03732	1.02232	0.13353	0.05259
	0.3	1.08545	1.05000	0.20143	0.06890
	0.4	1.15791	1.09047	0.27470	0.08060
	0.5	1.26268	1.14747	0.35824	0.08905
	0.6	1.41460	1.22825	0.46016	0.09542
	0.7	1.64398	1.34778	0.59632	0.10055
	0.8	2.02575	1.54342	0.80496	0.10491
	0.9	2.83041	1.95032	1.22217	0.10872
	0.99	6.65536	3.86672	3.14611	0.11177
	0.999	11.37400	6.22647	5.50649	0.11211
∞	0.1	1.01097	1.00670	0.07296	0.03230
	0.2	1.04384	1.02613	0.14461	0.05569
	0.3	1.10090	1.05873	0.21899	0.07219
	0.4	1.18812	1.10706	0.30079	0.08366
	0.5	1.31721	1.17668	0.39691	0.09177
	0.6	1.51114	1.27884	0.51972	0.09785
	0.7	1.82134	1.43906	0.69585	0.10275
	0.8	2.39524	1.73090	1.00005	0.10686
	0.9	3.93187	2.50381	1.78277	0.11034
	0.99	27.43928	14.26134	13.54756	0.11302
	0.999	253.47063	127.27735	126.56426	0.11324

The boundary collocation method is also used to solve for chains composed of N (various numbers up to 101) identical, equally spaced spherical particles translating along their centerline at the same velocity ($\beta_i = \beta$, $a_i = a$, $d_{i(i+1)} = d$, $U_i = U$, and $F_i^{(0)} = F^{(0)}$). Figure 3 plots the normalized drag forces $F_i/F^{(0)}$ of these chains as functions of the particle number i when $2a/d = 0.8$. These drag forces of the central spheres decline with increasing chain length, demonstrating that the sphere chain has a shielding effect. Near either end of the chain, the normalized drag forces on adjacent spheres change rapidly, exhibiting a significant end-of-chain effect. For relatively long chains, the drag forces of the central spheres change slowly with increasing chain length. In the limiting case of an infinitely long chain, the drag forces of all spheres are the same. The dashed curves in Figure 3 denote variation in drag force on sphere i as the number of spheres in the chain varies. As the chain length increases, these curves tend to flatten, further indicating the shielding effect in the sphere chain.

Table 5. Force correction parameters for the translation of three nonslip spherical particles ($\beta \to \infty$) with $a_1 = a_3$ and $d_{12} = d_{23} = d$.

a_1:a_2:a_3	$\frac{a_1+a_2}{d}$	h_{22}	$h_{11} = h_{33}$	$-h_{12} = -h_{32}$	$-h_{21} = -h_{23}$	$-h_{13} = -h_{31}$
1:2:1	0.1	1.00983	1.00545	0.04917	0.09834	0.02026
	0.2	1.03929	1.02173	0.09824	0.19647	0.03214
	0.3	1.08966	1.05016	0.14950	0.29899	0.03743
	0.4	1.16418	1.09429	0.20558	0.41117	0.03803
	0.5	1.26901	1.16107	0.27033	0.54066	0.03570
	0.6	1.41650	1.26414	0.35069	0.70138	0.03185
	0.7	1.63544	1.43408	0.46206	0.92413	0.02743
	0.8	2.01171	1.75859	0.64852	1.29703	0.02299
	0.9	2.95935	2.65310	1.11806	2.23612	0.01882
	0.99	16.93968	16.58526	8.10277	16.20554	0.01544
	0.999	150.91823	150.55899	75.09143	150.18287	0.01512
2:1:2	0.1	1.00965	1.00708	0.09597	0.04798	0.04554
	0.2	1.03833	1.02716	0.18718	0.09359	0.08402
	0.3	1.08812	1.05961	0.27808	0.13904	0.11793
	0.4	1.16515	1.10518	0.37360	0.18680	0.14954
	0.5	1.28216	1.16662	0.48116	0.24058	0.18114
	0.6	1.46540	1.25026	0.61446	0.30723	0.21499
	0.7	1.77511	1.37121	0.80418	0.40209	0.25322
	0.8	2.38539	1.57347	1.13797	0.56899	0.29787
	0.9	4.12485	2.06554	2.03080	1.01540	0.35129
	0.99	31.90236	9.06993	15.93593	7.96798	0.40955
	0.999	249.08712	63.37280	124.52991	62.26488	0.41607

Table 6. Force correction parameters for the translation of three spherical particles with $a_1 = a_3$, $d_{12} = d_{23} = d$, and $\beta a_2/\eta = 1$.

a_1:a_2:a_3	$\frac{a_1+a_2}{d}$	h_{22}	$h_{11} = h_{33}$	$-h_{12} = -h_{32}$	$-h_{21} = -h_{23}$	$-h_{13} = -h_{31}$
1:2:1	0.1	1.00529	1.00293	0.03525	0.07403	0.01528
	0.2	1.02113	1.01166	0.07026	0.14754	0.02582
	0.3	1.04797	1.02663	0.10601	0.22262	0.03232
	0.4	1.08703	1.04908	0.14361	0.30158	0.03553
	0.5	1.14051	1.08142	0.18448	0.38740	0.03622
	0.6	1.21237	1.12805	0.23082	0.48473	0.03515
	0.7	1.31037	1.19755	0.28675	0.60217	0.03295
	0.8	1.45273	1.30985	0.36170	0.75958	0.03014
	0.9	1.70095	1.53048	0.48690	1.02248	0.02706
	0.99	2.56400	2.39908	0.91753	1.92681	0.02427
	0.999	3.46300	3.33921	1.36686	2.87041	0.02400
2:1:2	0.1	1.00582	1.00439	0.07730	0.03623	0.03727
	0.2	1.02307	1.01696	0.15094	0.07075	0.07003
	0.3	1.05245	1.03726	0.22324	0.10464	0.09955
	0.4	1.09634	1.06544	0.29661	0.13903	0.12702
	0.5	1.15956	1.10238	0.37413	0.17538	0.15361
	0.6	1.25136	1.15012	0.46083	0.21602	0.18057
	0.7	1.39062	1.21308	0.56633	0.26547	0.20920
	0.8	1.62239	1.30195	0.71327	0.33435	0.24085
	0.9	2.09817	1.45253	0.97760	0.45825	0.27686
	0.99	4.11567	1.96502	2.00640	0.94052	0.31424
	0.999	6.76859	2.59103	3.33500	1.56315	0.31814

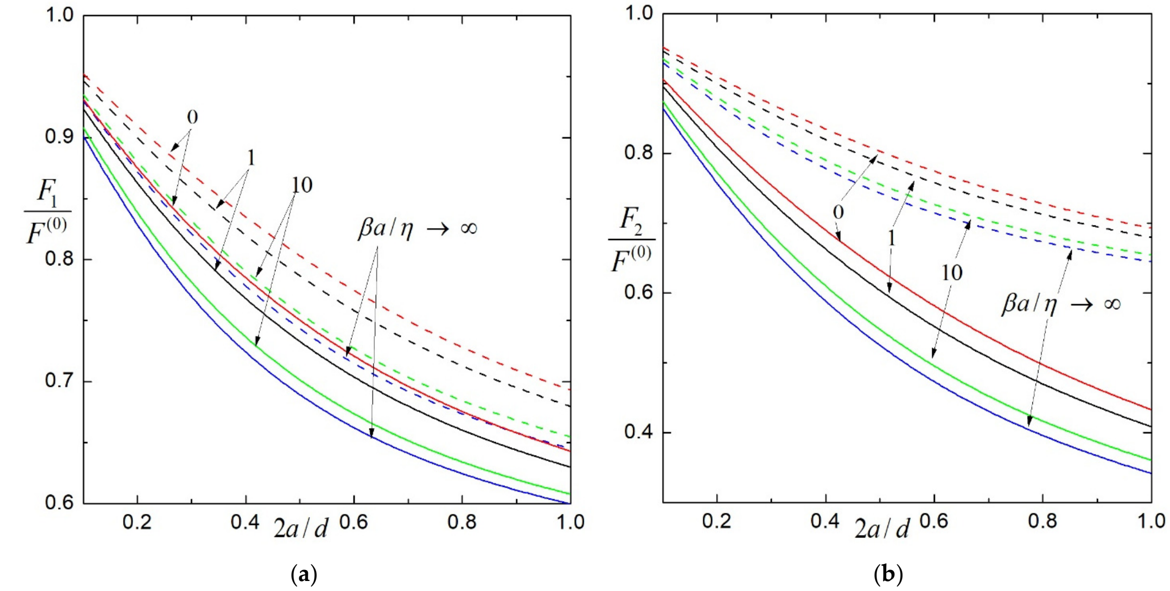

Figure 2. Normalized drag forces on three identical and equally spaced particles translating along their centerline at the same velocity versus spacing parameter $2a/d$ with several values of stickiness parameter $\beta a/\eta$: (**a**) the first (end) particle; (**b**) the second (central) particle. The dashed curves are plotted for the forces when only two particles are present for comparison.

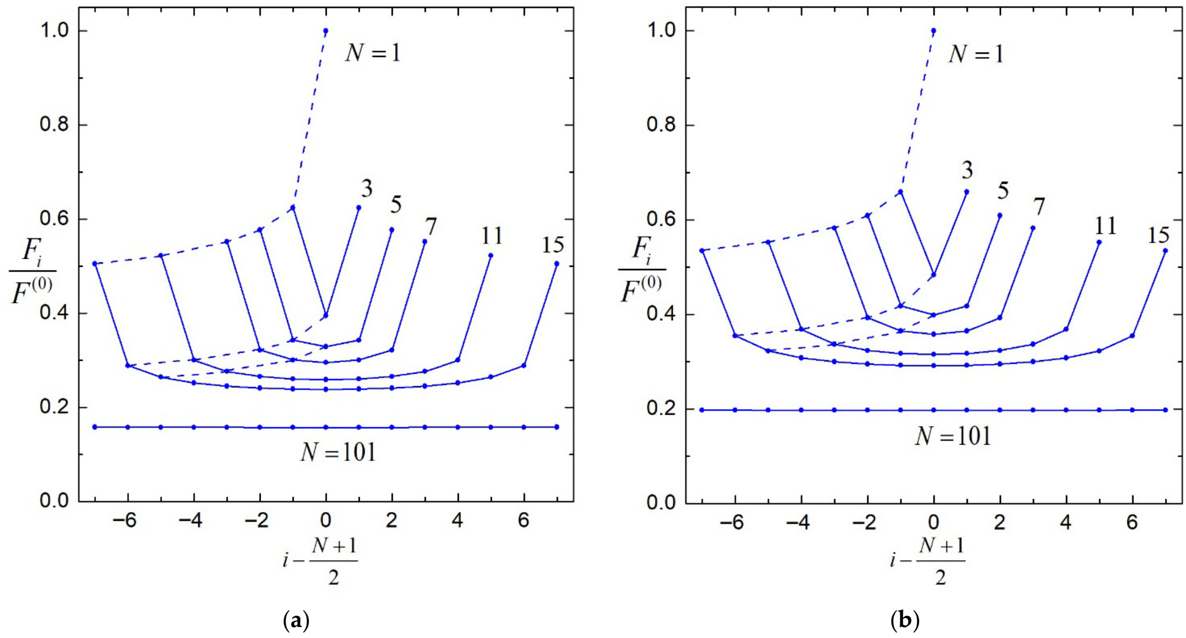

Figure 3. Normalized drag forces on N identical and equally spaced particles translating along their centerline at the same velocity versus particle number i with $2a/d = 0.8$: (**a**) $\beta a/\eta \to \infty$; (**b**) $\beta a/\eta = 1$.

Figure 4 shows the normalized drag forces $F_i/F^{(0)}$ as functions of the sphere number i in a chain of 9 identical, equally spaced spheres, where the particles translate at the same velocity, $2a/d = 0.8$, and various values of stickiness parameter $\beta a/\eta$ are considered. The results indicate that the drag force of each sphere declines as $\beta a/\eta$ increases. Namely, the interaction between particles is strongest for the nonslip sphere chain, while the interaction is weaker for a corresponding less sticky sphere chain.

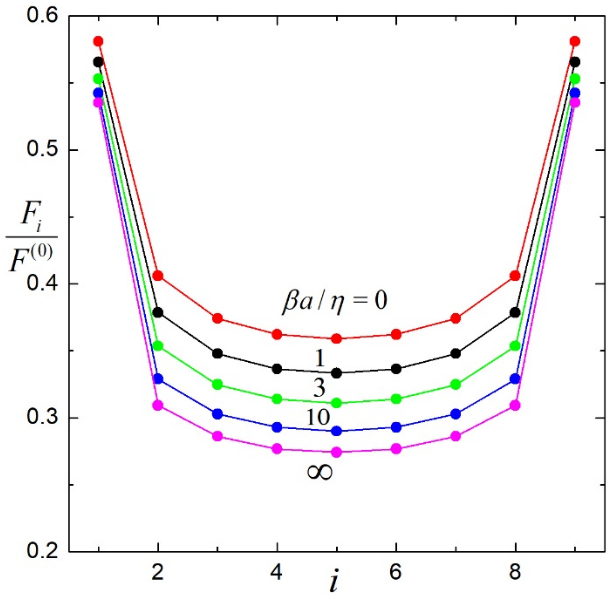

Figure 4. Normalized drag forces on 9 identical and equally spaced particles translating along their centerline at the same velocity versus particle number i with $2a/d = 0.8$ and several values of stickiness parameter $\beta a/\eta$.

To investigate the particle spacing effect, Figure 5 plots the relationship between the normalized drag force $F_i/F^{(0)}$ and sphere number i for a chain of 9 identical, equally spaced spheres translating at the same velocity, where $2a/d$ is a parameter. This figure shows the sphere chain under both nonslip ($\beta a/\eta \to \infty$) and partial-slip (with $\beta a/\eta = 1$) conditions. The results indicate that the end effect weakens as the particle spacing increases ($2a/d$ decreases). As expected, the drag force on each sphere declines as the particle spacing decreases.

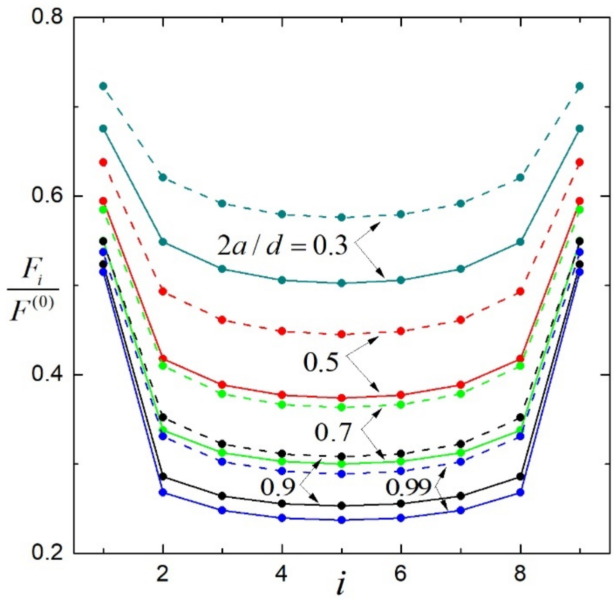

Figure 5. Normalized drag forces on 9 identical and equally spaced nonslip particles (solid curves, $\beta a/\eta \to \infty$) and partial-slip particles (dashed curves, with $\beta a/\eta = 1$) translating along their centerline at the same velocity versus particle number i with several values of spacing parameter $2a/d$.

5. Concluding Remarks

The pseudo-steady creeping flow induced by a linear chain of multiple slip spheres translating along their line of centers in a Newtonian fluid is examined. The particles are permitted to differ in radius, slip coefficient, velocity, and interparticle spacing. A semi-analytical solution of the Stokes equation is obtained using a boundary collocation method. Hydrodynamic interactions among the slip spheres are shown to be significant under appropriate conditions. For the two-sphere configuration, the calculated drag forces agree well with previously published numerical and asymptotic solutions. In the three-sphere case, the presence of a third particle substantially adjusts the forces acting on the other two, signifying noticeable many-body interaction effects. The interaction strength is more pronounced for smaller particles or those with lower slip coefficients. Calculations for longer particle chains further show a clear hydrodynamic shielding effect within the assemblage.

The results for the resistance problem have been given in the previous sections, in which the drag forces F_i on the chain of spheres at specified velocities U_i are calculated according to Equations (25) and (26). On the other hand, in the mobility problem, the forces acting on the spheres are known, and what needs to be determined are the resultant velocities of the particles. For the axisymmetric translation of N slip spherical particles, the velocity of sphere i can be expressed as

$$U_i = \sum_{j=1}^{N} m_{ij} U_{j0}, \qquad i = 1, 2, \ldots, \text{and } N, \tag{45}$$

with

$$U_{j0} = -\frac{\beta_j a_j + 3\eta}{6\pi\eta a_j(\beta_j a_j + 2\eta)} F_j, \tag{46}$$

which is the migration velocity of sphere j subject to applied force $-F_j$ in the absence of the others, and the mobility parameters m_{ij} are functions of the radii, slip coefficients, and separation distances of the spheres. For two spheres ($N = 2$), Equations (25), (26), (45) and (46) can be used to yield

$$m_{11} = (h_{11} - h_{12}h_{21}/h_{22})^{-1}, \tag{47}$$

$$m_{12} = (\frac{a_2}{a_1}) \frac{(\beta_2 a_2 + 2\eta)(\beta_1 a_1 + 3\eta)}{(\beta_1 a_1 + 2\eta)(\beta_2 a_2 + 3\eta)} (h_{21} - h_{11}h_{22}/h_{12})^{-1}, \tag{48}$$

while m_{22} and m_{21} can be similarly expressed by switching subscripts 1 and 2. These four mobility parameters can accordingly be calculated using the force correction parameters h_{11}, h_{12}, h_{21}, and h_{22} obtained in previous sections for the resistance problem.

The analytical solution developed in this study is limited to the slow motions of spheres at low Reynolds numbers. Although this article focuses on the motion of a simple axisymmetric finite linear array of sphere particles, the proposed solution method can be generalized to study the motion of arbitrary three-dimensional sphere assemblies [28]. This type of asymmetric problem could serve as a direction for future research.

Author Contributions: Conceptualization, H.J.K.; methodology, H.J.K. and W.C.L.; software, W.C.L.; formal analysis, H.J.K. and W.C.L.; investigation, H.J.K. and W.C.L.; writing—original draft preparation, H.J.K. and W.C.L.; writing—review and editing, H.J.K.; supervision, H.J.K.; funding acquisition, H.J.K. All authors have read and agreed to the published version of the manuscript.

Funding: This research was supported by the National Science and Technology Council of Taiwan under grant NSTC 113-2221-E-002-063-MY2.

Data Availability Statement: The original contributions presented in this study are included in the article. Further inquiries can be directed to the corresponding author.

Conflicts of Interest: The authors declare no conflicts of interest. The funders had no role in the design of the study; in the collection, analyses, or interpretation of data; in the writing of the manuscript; or in the decision to publish the results.

References

1. Stokes, G.G. On the effect of the internal friction of fluids on the motion of pendulums. *Trans. Camb. Phil. Soc.* **1851**, *9*, 8–106.
2. Pit, R.; Hervet, H.; Leger, L. Direct experimental evidence of slip in hexadecane: Solid interfaces. *Phys. Rev. Lett.* **2000**, *85*, 980–983. [CrossRef] [PubMed]
3. Tretheway, D.C.; Meinhart, C.D. Apparent fluid slip at hydrophobic microchannel walls. *Phys. Fluids* **2002**, *14*, L9–L12. [CrossRef]
4. Neto, C.; Evans, D.R.; Bonaccurso, E.; Butt, H.J.; Craig, V.S.J. Boundary slip in Newtonian liquids: A review of experimental studies. *Rep. Prog. Phys.* **2005**, *68*, 2859–2897. [CrossRef]
5. Choi, C.H.; Ulmanella, U.; Kim, J.; Ho, C.M.; Kim, C.J. Effective slip and friction reduction in nanograted superhydrophobic microchannels. *Phys. Fluids* **2006**, *18*, 087105. [CrossRef]
6. Alotaibi, M.A.; El-Sapa, S. Hydrophobic effects on a solid sphere translating in a Brinkman couple stress fluid covered by a concentric spherical cavity. *Phys. Fluids* **2024**, *36*, 033113. [CrossRef]
7. Chen, S.H.; Keh, H.J. Axisymmetric thermophoresis of multiple aerosol spheres. *Aerosol Sci. Technol.* **1996**, *24*, 21–35. [CrossRef]
8. Sharipov, F.; Kalempa, D. Velocity slip and temperature jump coefficients for gaseous mixtures. I. Viscous slip coefficient. *Phys. Fluids* **2003**, *15*, 1800–1806. [CrossRef]
9. Myong, R.S.; Reese, J.M.; Barber, R.W.; Emerson, D.R. Velocity slip in microscale cylindrical Couette flow: The Langmuir model. *Phys. Fluids* **2005**, *17*, 087105. [CrossRef]
10. Nir, A. Linear shear flow past a porous particle. *Appl. Sci. Res.* **1976**, *32*, 313–325. [CrossRef]
11. Chou, Y.F.; Keh, H.J. Axisymmetric slow rotation of coaxial soft/porous spheres. *Molecules* **2024**, *29*, 3573. [CrossRef]
12. Happel, J.; Brenner, H. *Low Reynolds Number Hydrodynamics*; Nijhoff: Dordrecht, The Netherlands, 1983.
13. Nashwan, M.G.; Ragab, K.E.; Faltas, M.S. Axisymmetric slow motion of a non-deformable spherical droplet or slip particle toward an orifice in a plane wall. *Phys. Fluids* **2022**, *34*, 083106. [CrossRef]
14. Tsai, M.J.; Keh, H.J. Slow rotation of coaxial slip colloidal spheres about their axis. *Colloids Interfaces* **2023**, *7*, 63. [CrossRef]
15. Chen, Y.C.; Keh, H.J. Slow motion of a spherical particle perpendicular to two planar walls with slip surfaces. *Fluids* **2025**, *10*, 287. [CrossRef]
16. Basset, A.B. *A Treatise on Hydrodynamics*; Dover: New York, NY, USA, 1961; Volume 2.
17. Wang, L.; Li, Z.; Wu, S.; Tao, S.; Zhang, K.; Bi, J.; Lu, G. Lattice Boltzmann simulation of neutrally buoyant circular slip particle motion in a clockwise double-lid-driven square cavity. *J. Appl. Phys.* **2023**, *134*, 214701. [CrossRef]
18. Anderson, J.L. Colloid transport by interfacial forces. *Ann. Rev. Fluid Mech.* **1989**, *21*, 61–99. [CrossRef]
19. Luo, H.; Pozrikidis, C. Interception of two spheres with slip surfaces in linear Stokes flow. *J. Fluid Mech.* **2007**, *581*, 129–156. [CrossRef]
20. Hocking, L.M. The effect of slip on the motion of a sphere close to a wall and of two adjacent spheres. *J. Eng. Math.* **1973**, *7*, 207–221. [CrossRef]
21. Reed, L.D.; Morrison, F.A. Particle interactions in viscous flow at small values of Knudsen number. *J. Aerosol Sci.* **1974**, *5*, 175–189. [CrossRef]
22. Chen, S.H.; Keh, H.J. Axisymmetric motion of two spherical particles with slip surfaces. *J. Colloid Interface Sci.* **1995**, *171*, 63–72. [CrossRef]
23. Keh, H.J.; Chen, S.H. Low Reynolds number hydrodynamic interactions in a suspension of spherical particles with slip surfaces. *Chem. Eng. Sci.* **1997**, *52*, 1789–1805. [CrossRef]
24. Saad, E.I. Motion of two spheres translating and rotating through a viscous fluid with slip surfaces. *Fluid Dyn. Res.* **2012**, *44*, 055505. [CrossRef]
25. Gluckman, M.J.; Pfeffer, R.; Weinbaum, S. A new technique for treating multi-particle slow viscous flow: Axisymmetric flow past spheres and spheroids. *J. Fluid Mech.* **1971**, *50*, 705–740. [CrossRef]
26. Chen, L.S.; Keh, H.J. The slow motion of coaxial droplets along their line of centers. *J. Chin. Inst. Chem. Eng.* **1992**, *23*, 53–66.

27. Jeffrey, D.J.; Onishi, Y. Calculation of the resistance and mobility functions for two unequal rigid spheres in low-Reynolds-number flow. *J. Fluid Mech.* **1984**, *139*, 261–290. [CrossRef]
28. Keh, H.J.; Tseng, Y.K. Slow motion of multiple droplets in arbitrary three-dimensional configurations. *AIChE J.* **1992**, *38*, 1881–1904. [CrossRef]